



HAL
open science

Non-symmetrical Bis-silylated Precursor Can (Also) Self-Direct the Assembly of Silsesquioxane Films

Lingli Ni, Abraham Chemtob, Céline Croutxe-Barghorn, Séverinne Rigolet, Irena Deroche, Laure Michelin, Loïc Vidal

► To cite this version:

Lingli Ni, Abraham Chemtob, Céline Croutxe-Barghorn, Séverinne Rigolet, Irena Deroche, et al.. Non-symmetrical Bis-silylated Precursor Can (Also) Self-Direct the Assembly of Silsesquioxane Films. Journal of Sol-Gel Science and Technology, 2017, 84, pp.222-230. 10.1007/s10971-017-4482-0 . hal-02442153

HAL Id: hal-02442153

<https://hal.science/hal-02442153>

Submitted on 16 Jan 2020

HAL is a multi-disciplinary open access archive for the deposit and dissemination of scientific research documents, whether they are published or not. The documents may come from teaching and research institutions in France or abroad, or from public or private research centers.

L'archive ouverte pluridisciplinaire **HAL**, est destinée au dépôt et à la diffusion de documents scientifiques de niveau recherche, publiés ou non, émanant des établissements d'enseignement et de recherche français ou étrangers, des laboratoires publics ou privés.

1 Non-symmetrical Bis-silylated Precursor Can (Also) Self-
2 Direct the Assembly of Silsesquioxane Films

3 *Lingli Ni,^{#*} Abraham Chemtob,^{†*} Céline Croutxé-Barghorn,[‡] Séverinne Rigolet,[†] Irena Deroche,[†]*
4 *Laure Michelin,[†] Loïc Vidal[†]*

5 [#] Key Laboratory for Palygorskite Science and Applied Technology of Jiangsu Province, College of
6 Chemical Engineering, Huaiyin Institute of Technology, Huaian 223003, People's Republic of China

7 [†] Institute of Material Science of Mulhouse, CNRS, UMR 7361, University of Haute-Alsace, 3 bis rue
8 Alfred Werner 68093 Mulhouse Cedex, France

9 [‡] Laboratory of Photochemistry and Macromolecular Engineering, ENSCMu, University of Haute-
10 Alsace, 3 bis rue Alfred Werner 68093 Mulhouse Cedex, France

11
12 ***Corresponding authors:**

13 Dr. Abraham Chemtob; E-mail: abraham.chemtob@uha.fr; Tel: +33 3 8960 8834

14 Dr. Lingli Ni; E-mail: ningli520@126.com; Tel: +86 517 8355 9056; Fax: +86 517 8355 9056

15

16 **Abstract:**

17 Symmetric α,ω -bis-silylated precursors are the standard building blocks of self-assembled bridged
18 silsesquioxanes, a unique class of robust ordered nanomaterials prepared by sol-gel process without external
19 surfactant. We report an unprecedented approach based on the utilization of a dissymmetric bis-silylated
20 precursor, 1,2-bis(trimethoxysilyl)decane (**1**), in which the two alkoxy groups are carried by adjacent methylene
21 groups. Extensive characterization — based on X-ray diffraction, real-time FTIR, electron and optical
22 microscopy, ^{29}Si solid-state NMR, thermogravimetry, and molecular modeling — shows surprisingly that such
23 non-symmetrical precursor is highly conducive to achieve highly ordered lamellar mesostructure, able to sustain
24 temperature up to 120 °C. To emphasize the effect of the alkoxy group functionality and position, comparison is
25 made systematically with analogous silsesquioxanes derived from bis-(**2**) and mono-silylated (**3**) precursors. The
26 sol-gel polymerization of **1** is unique by its ability to produce a homogeneous film possessing structural
27 characteristic on multiple scales: uniform microcrystallites consisting of nanolamellar organosilica hybrid
28 material. The most likely mesostructure consists of bilayers of slightly interpenetrated *trans* C_8H_9 chains, with a
29 single central siloxy-hydrocarbon chain $(\text{Si}_2\text{O}(\text{OH})_4\text{-C}_2\text{H}_3)_n$. To permit a good lateral chain packing, the
30 hydrocarbon chain of two adjacent silicon atoms point in opposite directions.

31
32 **Keywords:** self-assembly, silsesquioxane, non-symmetric, photopolymerization, template-free, alkoxy silane

33
34

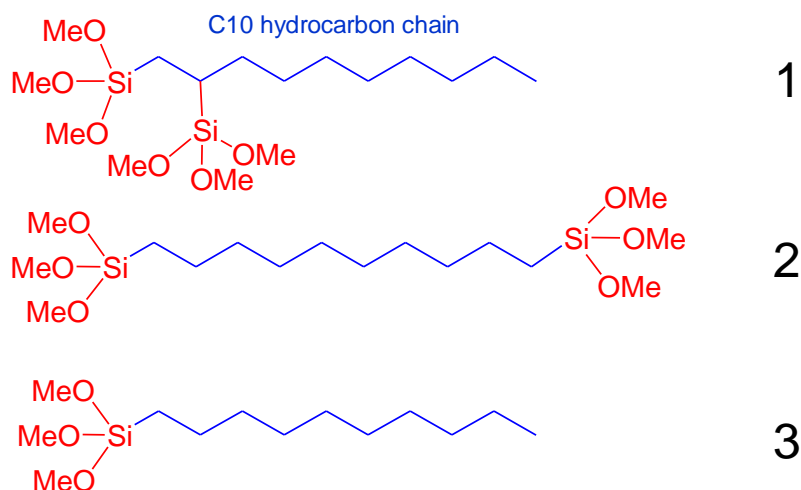
35 1. Introduction

36 One of the frontiers in materials chemistry is the design of robust polymer structures with nanometer size
37 organization [1]. Of high interest is their potential to improve and tune properties such as mechanical strength [2]
38 or permeability [3], which are highly dependent on local order and geometry. Among the different
39 nanostructuring routes possible, polymerization within Lyotropic Liquid Crystal (LLC) mesophases has been
40 currently recognized as one of the simplest conceptually, and also the most suitable for scaling-up [4]. In this
41 field, sol-gel polymerization of alkoxy silane precursors is undeniably the most successful example [5]. In
42 combination with supramolecular self-assembly, this step-growth process has been extensively used to
43 produce a full range of robust siloxane-crosslinked ordered nanomaterials [6, 7]. Generally, the LLC
44 mesophases originate from an external surfactant (macro)molecule with the additional cooperative interaction of
45 alkoxy silane ($\text{Si}(\text{OR}')_4$) or organoalkoxy silane ($\text{R}_n\text{-Si}(\text{OR}')_{4-n}$) species.

46 To drive self-assembly, it is now established that a templating species such as surfactant can be obviated,
47 but at the cost of molecular design to achieve alkoxy silane precursors able, alone, to self-organize [8, 9]. Since
48 the discovery on the late 1990s that long chain *n*-alkylalkoxy silane can self-assemble spontaneously during sol-
49 gel polymerization [10], a wealth of precursors endowed with the same self-organization capacity has been
50 released [11-13]. However, their self-directed self-assembly has been much less documented than that of
51 conventional amphiphiles. Today, the necessary and sufficient structural factors at the molecular level that
52 govern their self-assembly ability are not well identified because of different challenges. Firstly, these specific
53 organosilanes reveal generally their amphiphatic structure – and thus their self-assembling ability – only after
54 hydrolysis of the lyophobic alkoxy silyl groups into lyophilic silanol groups [14]. Additionally, the resultant
55 amphiphatic silicic acid species ($\equiv\text{Si-OH}$) generated in situ remain ill-defined and transient. Consequently, they
56 do not display a clearly defined phase behavior compared to conventional surfactants, and are difficult to isolate
57 because subjected to irreversible condensation reactions to form stable siloxane bonds [15, 16]. Last but not
58 least, alkoxy silane self-directed self-assembly is not only a question of precursor design, because this process
59 strongly relies also on environmental conditions (relative humidity, temperature...), processing parameters
60 (catalyst, solvent, dilution...), as well as on sol-gel condensation rates [17].

61 Today, most of the research on precursor design has been focused on telechelic α,ω -bis-silylated linear
62 precursors ($(\text{R}'\text{O})_3\text{Si-R-Si}(\text{OR}')_3$) carrying reactive ethoxy or methoxy silyl groups at each extremity. It is
63 generally agreed that such symmetrical architecture may drive close packing and weak interactions (such as van
64 der Waals, π - π stacking and H-bonding, etc.) between side-by-side organic moieties [12, 18, 19]. End-to-end
65 linking reaction takes place eventually to lock in the mesostructure through siloxane bonds' formation, in a
66 manner which is compliant with the preorganized chain template. Recent studies were instrumental in shedding
67 light onto the complex structuring mechanism [20, 21]. Although the literature reports a number of self-
68 assembled organosilica derived from mono-silylated precursors $(\text{R}'\text{O})_3\text{Si-R}$ [11, 13, 22], the originality relies
69 less on the alkoxy group architecture, and much more on the variety of bridging or pendant organic lyophobic
70 groups in terms of chemical composition [23], length [24, 25], branching [26] or unsaturation [27]. However,
71 there are many questions arising on the influence of the position of the single or multiple $\text{Si}(\text{OR}')_3$ groups along
72 the organic chain R, their functionality, the introduction of branching, because all these structural factors are able
73 to affect sol-gel reactivity, solubility of the hydrolyzed species, the nature of the LLC mesophases, or the

74 packing of the precursor molecules [28]. Recently, efforts have been made by Kuroda and coworkers to
 75 investigate more complex precursor architectures by replacing the monomeric $-\text{Si}(\text{OR}')_3$ extremities by pre-
 76 designed branched or cubic multisiloxane units [29-32]. The net effect was a decrease of the mesophase packing
 77 parameter (because of the higher volume of the hydrophilic head), and higher curvature's aggregates exhibiting
 78 hexagonal or cubic organization were synthesized.



79
 80 **Scheme 1.** Structure of the three C_{10} -based trimethoxysilane precursors: **1**, **2** and **3**.

81
 82 In this study, we report a very promising and unprecedented approach based on the utilization of a
 83 dissymmetric linear bis-silylated precursor: 1,2-bis(trimethoxysilyl)decane (**1**, see structure in **Scheme 1**).
 84 Previous works showed that dissymmetric precursors were useful to fabricate mesoporous periodically ordered
 85 organosilica (POM) structures but only through a surfactant-templated process [33, 34]. In **1**, the two
 86 methoxysilyl groups are no longer located at opposite ends of the hydrocarbon chains, but carried by two
 87 adjacent methylene groups, thereby inducing a dissymmetric structure. Breaking the symmetry is likely to
 88 change molecule polarizability, interfacial and self-assembling properties, and possibly the type and level of
 89 organization. After hydrolysis, the organosilane **1** will contain two hydrophilic groups ($\text{Si}(\text{OH})_3$) connected by a
 90 short linkage ($-\text{CH}_2-\text{CH}_2-$), as well as a single hydrophobic group (C_8H_{17}). Therefore, its structure resembles that
 91 of gemini surfactant [35, 36]. These dimeric surfactants, having generally two hydrophobic tails, stand out by
 92 their unique properties compared to conventional surfactant: lower critical micelle concentration, higher surface
 93 activity, unusual aggregation behavior [37]. To emphasize the effect of alkoxy group architecture, the self-
 94 assembly of **1** was systematically compared with that of two other homologues shown in Scheme 1, and based
 95 on a similar straight chain of 10 carbons: a symmetric analogue **2** (1,10-bis(trimethoxysilyl)decane, $(\text{H}_3\text{CO})_3\text{Si}-$
 96 $\text{C}_{10}\text{H}_{20}-\text{Si}(\text{OCH}_3)_3$), and a mono-silylated analogue **3** (*n*-decyltrimethoxysilane, $(\text{H}_3\text{CO})_3\text{Si}-\text{C}_{10}\text{H}_{21}$).

97 We report herein extensive characterization — based on X-ray diffraction, real-time FTIR, transmission
 98 electron microscopy, polarized optical microscopy, ^{29}Si solid-state NMR, thermogravimetry, and molecular
 99 modeling — showing that the dissymmetrical architecture of **1** is highly conducive to achieve highly ordered
 100 organosilica lamellar mesostructure. To compare the self-assembly of these three precursors, we used a sol-gel
 101 photoprocess, a UV light-induced inorganic polymerization developed by our group since 2011 [38]. Based on a
 102 conventional hydrolytic mechanism, it relies on photoacid-catalyzed hydrolysis and condensation reactions

103 starting from a solvent-free liquid precursor (**1-3**) deposited as thin films and containing only a photoacid
104 generator (see experimental section for details).

105

106 **2. Experimental section**

107 *2.1. Chemicals*

108 1,2-bis(trimethoxysilyl)decane (**1**, 95 % mol.) and *n*-decyltrimethoxysilane (**3**, 95 % mol.) were supplied by
109 ABCR. 1,10-bis(trimethoxysilyl)decane (**2**, 95 % mol.) was purchased from SiKÉMIA. Photoacid generator
110 UV1241 (bis-dodecyl diphenyliodonium hexafluoroantimonate salt) was provided by Deuteron. All of the
111 chemicals were used as received.

112 *2.2. Synthesis of hybrid films derived from alkylsilane precursors (1-3)*

113 In a typical procedure, photoacid generator (UV1241, 0.5 % wt.) was dissolved in the alkoxy silane
114 precursor (**1-3**) to form a photolabile solution in the absence of UV light. Then the resultant formulation was
115 deposited on a silicon wafer using an Elcometer 4340 automatic film applicator equipped with a wire wound bar
116 to produce a ~2 μm thick liquid film. Sol-gel photoinduced polymerization was performed at room temperature
117 under the polychromatic light of a medium pressure mercury-xenon lamp (Hamamatsu, L8251, 200 W, 365 nm
118 reflector) coupled with a flexible light-guide, with an incident light intensity adjusted at 20 mW cm^{-2} . The
119 samples were irradiated 1800 s to yield solid polysilsesquioxane hybrid film with minimal temperature increase
120 at the film surface ($< + 3$ °C). During UV irradiation, the room humidity was also maintained between 50 and
121 55%. Note that the as-synthesized films were never heated.

122 *2.3. Characterization*

123 The resulting samples were characterized by a range of techniques: time-resolved FTIR, X-ray diffractions
124 (XRD), polarized optical microscopy (POM), transmission electron microscopy (TEM), ^{29}Si solid state NMR,
125 thermogravimetry (TGA). FTIR spectra were recorded in real time mode during irradiation with a Bruker Vertex
126 70 spectrophotometer equipped with a MCT detector. The resolution of the infrared spectra was 2 cm^{-1} . Small
127 angle XRD were obtained on a PANalytical θ - θ mounting X'pert Pro MPD diffractometer with fixed slits using
128 $\text{Cu/K}\alpha$ radiation ($\lambda = 1.5418$ Å). Before analysis, films on silicon wafers were directly deposited on a stainless
129 steel sample holder. Data were collected between 1 and 10° 2θ degrees with a scanning step of 0.017° s^{-1} . The
130 evolutions of the XRD patterns with temperature were followed, on scratched film, on a PANalytical θ - 2θ
131 mounting X'Pert PRO MPD diffractometer ($\text{Cu/K}\alpha$ radiation: $\lambda = 1.5406$ Å) and equipped with an Anton Paar
132 HTK1200 heating chamber in flat plate reflection geometry (sample cup made of Al_2O_3). Both diffractometers
133 were equipped with an X'Celerator real-time multiple strip detector. The TEM observations were performed
134 with a Philips CM200 microscope operating at 200 kV. The powders were deposited at the surface of copper
135 observation grids directly. The ^{29}Si Cross Polarization Magic Angle Spinning (CP-MAS) solid state NMR
136 spectra was performed on a Bruker Avance II 300 spectrometer with a Bruker double channel 7 mm probe at a
137 Larmor frequency of 79.48 MHz. Spectra were recorded with a recycling delay of 10 s, a spinning frequency of
138 4 kHz and a contact time of 4 ms, using a ramp for Hartmann-Hahn matching and a high-power proton
139 decoupling during the acquisition ^1H spin-lattice relaxation times (T_1) were measured with the inversion-
140 recovery pulse sequence for all samples. ^{29}Si chemical shift is relative to tetramethylsilane. Birefringent

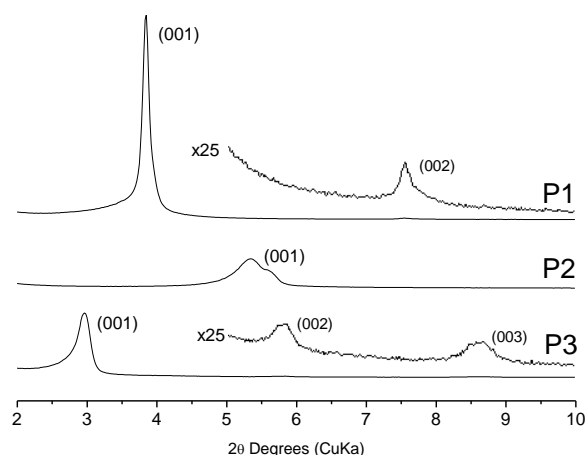
141 properties of the UV-cured films were investigated by a polarized optical microscope of Olympus BX51-P. The
142 microscopic structures of the synthesized silsesquioxanes were built from scratch on the basis of the X-ray
143 diffraction pattern, using the Materials Studio Simulation Package. The geometries of considered structures were
144 optimized through the classical molecular mechanics energy minimization procedure. We achieved the energy
145 minimization using the Forcite module included in Material Studio Simulation Package with the quasi Newton-
146 Raphson minimization algorithm and convergence criterions of 1.0×10^{-5} kcal/mol for the energy tolerance and
147 1.0×10^{-4} kcal/mol/Å for the residual force tolerance. The interactions between the system constituting atoms are
148 described through Dreiding force field parameters [39], well suited for hybrid solid systems. No specific
149 constraints were imposed to the structure optimizations.

150

151 3. Results and discussion

152 The three organosilica hybrid films **P1**, **P2** and **P3** derived respectively from **1**, **2** and **3** were analyzed by
153 XRD to assess their mesoscopic organization. Only the symmetrical bis-silylated precursors **2** and its mono-
154 silylated analogue **3** have been used in the past for the preparation organosilica hybrid materials by conventional
155 sol-gel process, but in any case, amorphous products were reported [40-43]. Because of too short alkylene
156 spacers, the cohesive forces between organic moieties are considered insufficient to drive self-assembly. By
157 contrast, in our case, all samples showed clear indications of mesostructuring after UV irradiation as is evident
158 from the XRD patterns displayed in **Figure 1**. Remarkably, the XRD pattern of **P1** obtained from the
159 dissymmetric bis-silylated derivative exhibited two sharp and intense Bragg peaks at 3.84° and 7.58° 2θ with
160 associated d spacing distance of 23.0 Å and 11.6 Å, respectively. These peaks were straightforwardly indexed as
161 the (001) and (002) directions of a lamellar structure with a basal spacing of 23.0 Å, indicative of a long range
162 periodic ordering. Surprisingly, **P2** prepared from the symmetric bis-silylated precursor resulted in a single broad
163 and weak Bragg diffraction at 5.34° , indicative of a lower level of ordering. Conversely, **P3** demonstrated also an
164 ability to self-assemble since its XRD pattern showed three harmonics at 2.96° (29.5 Å), 5.79° (15.1 Å) and 8.62°
165 (10.1 Å), although the peaks were less intense and broader than in **P1**. In **P3**, the interlamellar distance of 29.5 Å
166 closely corresponds to the theoretical value of 29.6 Å predicted for the bilayer structure, $\text{CH}_3(\text{CH}_2)_9\text{SiO}_x\text{---}$
167 $\text{O}_x\text{Si}(\text{CH}_2)_9\text{CH}_3$, from molecular models with a fully extended length of 30.0 Å for each alkylsiloxane unit (see
168 last section on molecular modelling for details). Regarding **P1** (23.0 Å), the intense diffraction peak at a 2θ value
169 of 7.58° corresponds obviously to the lamellar ordering along the c-axis, but the d-spacing of 23.0 Å cannot be
170 related to the length of the organic unit. This is the reason why a complete molecular modelling study was
171 performed in the last section.

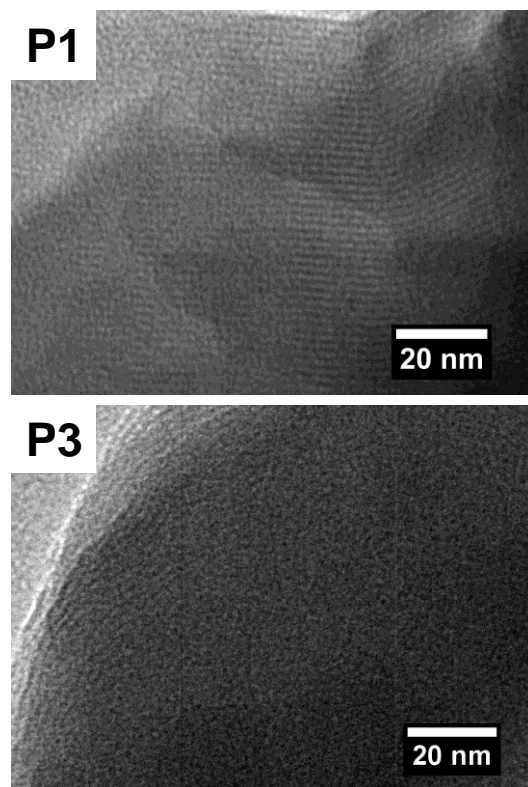
172



173
 174 **Figure 1.** Experimental small angle X-ray diffraction patterns of UV-irradiated hybrid films: **P1**, **P2** and **P3** and
 175 their structural models.
 176

177 Firstly, it may be inferred from XRD data that introducing a dissymmetry in the bis-silylated precursor
 178 architecture can be an effective means to achieve a higher level of ordering. Secondly, this change does not
 179 affect the type of mesostructure which remains of lamellar-type, currently the most reported mesophase for self-
 180 directed organosilica systems [13]. Thirdly, there is the confirmation that sol-gel photopolymerization is a
 181 relevant method for creating a regular assembly of organic and inorganic moieties by offering optimal reaction
 182 conditions for LLC templating as discussed in a separate publication [44]. To highlight the key features:
 183 thermodynamically, photopolymerization is optimal for mesophase formation because it is conducted at ambient
 184 temperature, without organic solvent. In addition, spatial control enables to irradiate in a closed chamber
 185 allowing the control of the relative humidity (55 % in these experiments), which is a critical parameter in silica
 186 thin film self-assembly. Finally, optimal control of light irradiance (20 mW cm^{-2}) enables maintaining fluidity on
 187 a larger timescale to prevent the system from “freezing” at an intermediate disordered state, while achieving
 188 relatively fast solid film formation (30 min irradiation)

189 Further proofs of the periodic mesostructuration of the hybrid films **P1** and **P3** were provided by electron
 190 microscopy. The TEM images of **Figure 2** confirmed the layered morphology presumably consisting of stacks of
 191 organic chains layers and $\text{SiO}_x(\text{OH})_y$ sheets identified by their slight difference of contrast. The stripes were
 192 particularly well-defined in the case of **P1**, providing an additional evidence of its high level of organization. The
 193 interlamellar distance of 2.3 nm and 2.9 nm found respectively in **P1** and **P3** were in accordance with the values
 194 obtained by XRD. Also noteworthy is that it was not possible to detect some organized regions by TEM in the
 195 sample **P2**, agreeing with the fact that self-assembly probably involves a very minor fraction of this sample.
 196



197
198 **Figure 2.** TEM image of **P1** and **P3** films.
199

200 Hybrid films' birefringent properties were also examined by POM. For all precursors, the initial liquid films
201 were completely dark, suggesting an isotropic behaviour. Unlike **P2**, **P1** and **P3** both showed birefringent
202 domains under crossed polarizers, indicative of an anisotropic organization. Remarkably, the **P1** crystal grew as
203 thin and well-defined needles, which were visible only under polarised light. The dimensions of a typical
204 microscopic crystallite of **P1** were approx. 10-100 μm in length, and 5 μm in width. When the long axis was
205 parallel to the polarizer or analyzer, each needle displayed a very strong and uniform birefringence with a perfect
206 optical extinction, implying that each needle is associated with a single crystal. This result agrees with a hybrid
207 material of controlled and homogeneous morphology (film) possessing structural characteristic on multiple
208 scales: well-defined and uniform microcrystallites consisting of nanolamellar organosilica hybrid material. In
209 contrast, **P3** film revealed under polarised light many bright submicrometer particle-like features devoid of
210 uniform microcrystal. This result indicates a very different crystallization process, resulting in the formation of
211 non-uniform microdomains of different sizes randomly distributed in the film, which is relatively common with
212 ordered organosilica hybrid materials [45].
213

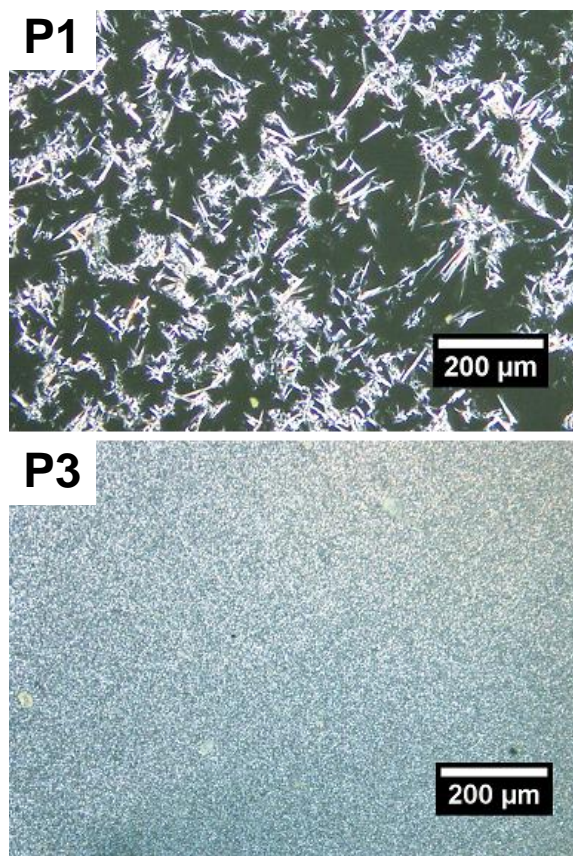


Figure 3. Microscopy images in polarized light of **P1** and **P3** hybrid films

214

215

216

217

218

219

220

221

222

223

224

225

226

227

228

229

230

231

232

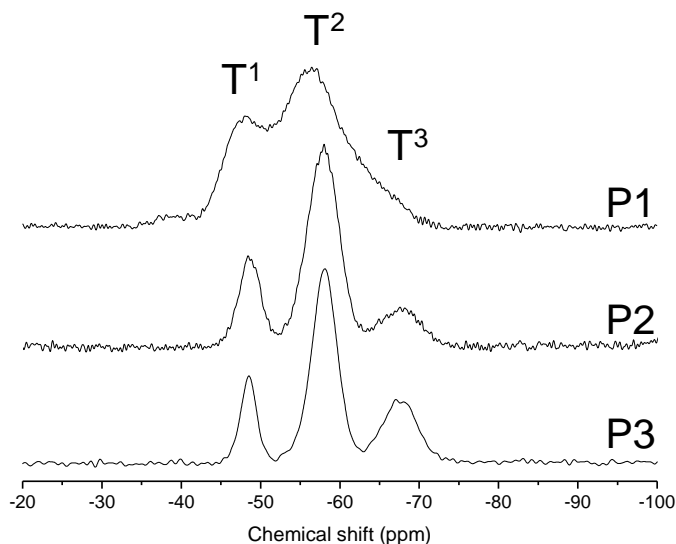
233

234

235

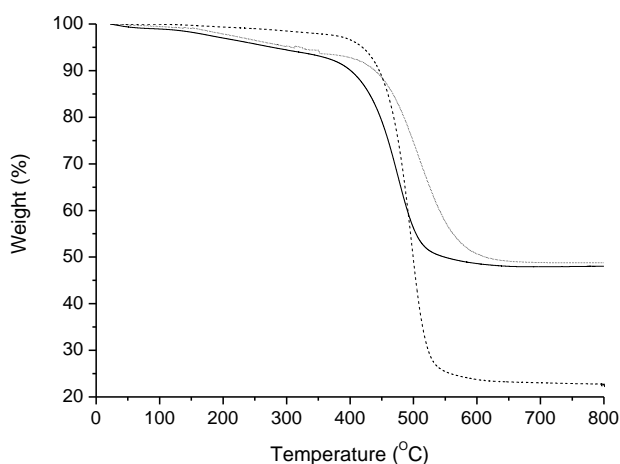
²⁹Si CP MAS NMR spectroscopy indicates that the as-synthesized films were composed of condensed and completely hydrolysed silsesquioxane. As illustrated in **Figure 4**, the spectra were dominated by T² siloxane species (OH(R)Si(OSi)₂, -58 ppm) with the following order of condensation: **P3** > **P2** > **P1**. Exact values for the degree of condensation are not purposely provided because CP measurement can minimize the proportion of T3 sites as these latter have no nearby hydrogens from which to cross-polarise. Nevertheless, a comparison between these samples obtained under similar acquisition conditions is perfectly correct. In **P1**, the spatial proximity between the two reactive Si(OR³) groups results in a greater steric hindrance that reduces the sol-gel reactivity, accounting for the lower degree of condensation. Broad lines are found in all instances, which reflect the amorphous state of the siloxane network. Such result is expected since the crystallinity in self-assembled organosilica only arises from the periodicity of the organic units. More intriguing, however, was the strong broadening of the resonances found with **P1**, informative of possibly more rigid segments compared to other samples. For **P1**, the higher degree of order (see XRD data) is consistent with a more homogeneous distribution of isotropic chemical shifts (Si feels a chemically similar environment) which should contribute conversely to line narrowing because of the higher mobility induced by self-assembly. The opposite result clearly states that in ²⁹Si CP MAS spectrum the dominant interactions must be different: dipolar interactions (which are not completely suppressed), and more probably the intrinsic mobility of the siloxane chains. Therefore, it can be hypothesized that complex motional effects may contribute to the line widths of the silicon CP MAS spectrum of **P1**. While the silicon atoms form generally a single siloxane (SiO)_n backbone in lamellar organosilica hybrids (**P2-3**), we assume that a different chemical environment can arise in **P1** leading to formation of a hybrid ((SiO-

236 C₂H₄)_n), motionally more restricted central chain. This different chemical structure is fully presented in the
237 molecular modelling section below. Additionally, because of the precursor's dissymmetric structure, the 2
238 silicon atoms are likely to display distinct chemical shifts which may account for broadness the resonances.
239



240
241 **Figure 4.** Solid state ²⁹Si CP MAS NMR spectra of UV cured hybrid films **P1**, **P2** and **P3**

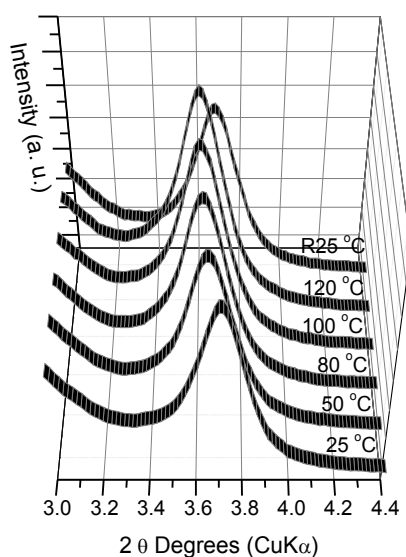
242
243 **Figure 5** displays TGA plots of the three organosilica hybrid materials obtained under nitrogen, supporting
244 their high thermal stability. Regardless of the precursor, three discernible weight loss regions were observed: (I)
245 a small one below 150 °C due to the loss of physically bound water, (II) a second one at 150 - 400 °C because of
246 the loss of water released from the condensation reactions between unreacted SiOH groups and (III) a large
247 weight loss after 400 °C due to the decomposition of alkylene groups in the hybrid materials, presumably leaving
248 a stable SiO_x residue. Clearly, siloxane cross-linking provides a significant thermal stability to these three hybrid
249 films.



250
251 **Figure 5.** Thermal gravimetric analysis of the UV-cured hybrid films under N₂ flow: **P1** (—), **P2** (...), and **P3** (---)

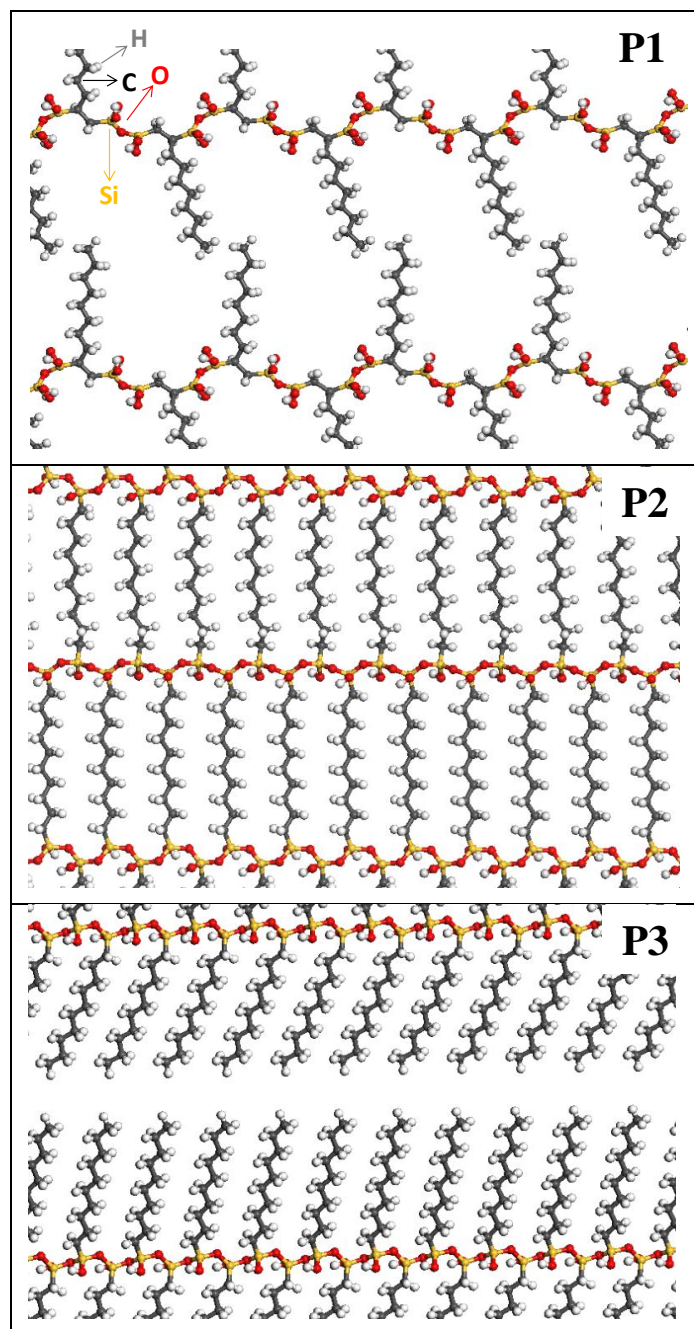
252
253 Additionally, it is also important to assess whether the silsesquioxane organization can be preserved upon
254 heating. To reply to this question, **Figure 6** displays a series of thermoXRD patterns of **P1** monitored in situ in

255 the 2θ range (between 3.00° to 4.40° 2θ range) to show the evolution of the 001 reflection when temperature is
 256 increased in the measurement enclosure. By increasing temperature from 25°C to 120°C , the 001 peak only
 257 slightly shifts to lower angles (from 3.71° to 3.64° 2θ) translating an extension of the interlamellar distance, but
 258 without any signal broadening as assessed by a steady Full Width at Half Maximum (FWHM) value of 0.26° .
 259 More interestingly, cooling back to room temperature leads the 001 reflection to return to its initial position,
 260 providing strong evidence of a high thermal stability. Other experiments (not reported) supported the stability of
 261 **P1**'s crystalline mesostructure during a 1 h heating at 100°C or after a 1h immersion in acetone. By contrast, **P3**
 262 became amorphous (as exemplified by the disappearance of the sharp diffraction peaks) for a threshold
 263 temperature as low as 46°C , similarly to reported results of hexadecyl silsesquioxane hybrids [46-48]. Such
 264 difference can be ascribed to the higher level of ordering of **P1**, with stronger cohesive forces inside the
 265 supramolecular materials hindering the thermal disordering of the product.

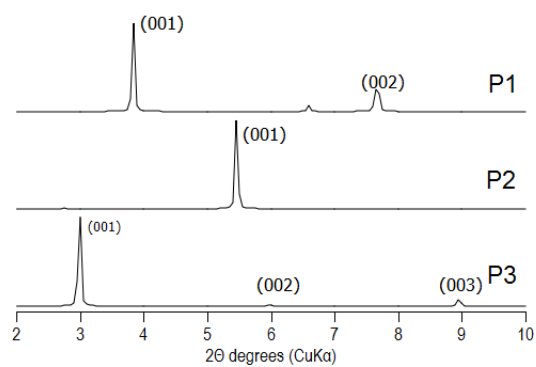


266
 267 **Figure 6.** In-situ thermo XRD patterns with 001 reflections of UV-cured **P1** film for different temperatures up to
 268 120°C (R25°C refers to the sample returning to 25°C after heating)
 269

270 The structural models of **P1**, **P2** and **P3** were designed using molecular mechanics simulation with the
 271 Dreiding force field. For sake of simplicity, our models shown in **Figure 7** were built as stacked planar
 272 structures, resulting from 2D monomers interlinking. However, the existence of siloxane bonds between two Si
 273 atoms arranged in parallel opposite planes could be also envisaged. Regardless of the precursors, there is a good
 274 agreement between the experimental XRD data and the simulated XRD spectra associated to the structural
 275 models (**Figure 8**). As depicted in Figure 7, **P2** and **P3** display the conventional structural features of ordered
 276 mono- and bridged lamellar silsesquioxane [49]. Arising from the mono-silylated precursor, **P3** consists of
 277 bilayered stacks of highly trans $\text{C}_{10}\text{H}_{21}$ chains, with a single Si-O-Si backbone. The alkyl chains carried by two
 278 adjacent silicon atoms point in opposite direction so as to avoid steric hindrance (meaning that half of the silicon
 279 atoms have chains pointing upward while the other half have chains pointing downward) [50]. **P2**, or rather the
 280 ordered fractions of **P2**, consists of alternating stacks of $\text{C}_{10}\text{H}_{20}$ bridging groups connected to a single siloxy
 281 chain. Again, this staggered packing arrangement is present since the Si-O-Si bond distance is too short to
 282 accommodate all-trans alkyl chains due to repulsive interactions between adjacent chains.



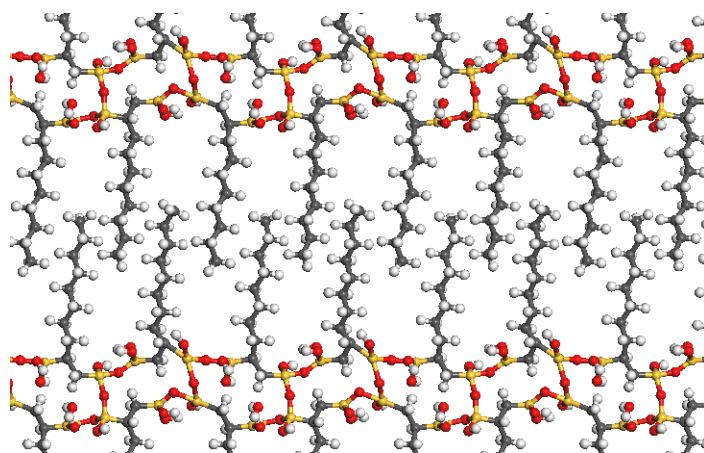
283 **Figure 7.** Simulated structure models of UV cured hybrid films **P1**, **P2**, **P3**



284
285 **Figure 8.** Simulated small angle X-ray diffraction patterns of the 3 structural models **P1**, **P2** and **P3** presented in
286 Figure 7.

287 It is really with **P1** that the added value of molecular modelling emerges. In this latter case, we propose as
288 the most likely mesostructure a bi-layered stack of slightly interpenetrated highly *trans* C₈H₁₇ chains, with a
289 single central hybrid siloxy-hydrocarbon (Si₂O(OH)₄-C₂H₃)_n backbone. In this structure the large inter chain
290 spacing provides a better stability and enables to achieve periodicity on long range order. Interestingly, the
291 hybrid nature of the central chain comes from the interlinking of dissymmetric monomers, which imposes the
292 presence of T¹ siloxane species in the present 2D structure (T² can also exist by condensation reaction between
293 two opposite Si atoms belonging two separate planes, not represented in Figure 7). By contrast, **P2** and **P3** show
294 a central siloxy sheet based on T² siloxane species. Interestingly, such result is in agreement with the ²⁹Si NMR
295 data, highlighting **P1** as the less condensed mesostructure. In a previous work, Dieudonné also emphasized the
296 detrimental effect of a high condensation's degree on structural ordering [15]. The fact that the central chain is
297 not only composed of flexible siloxane bonds but comprises Si-CH₂ bindings may lead to mobility restrictions,
298 consistent with the broader NMR resonances of silicon CP-MAS spectrum. There is also an increased free
299 volume available to the chains as the result of increased distance between the alkyl chains. Clearly, other
300 structural models of **P1** matching the inter-lamellar spacing given by XRD — can be also designed but are not
301 physically possible. An illustrative example is displayed on **Figure 9**. This alternative model corresponds to a
302 partially interpenetrated system, exhibiting inter-chain distances as short as 3.0 Å, resulting in steric hindrance
303 between shortest hydrogen atoms of distinct alkyl chains, separated by a distance inferior to 1.5 Å. Consequently,
304 energy minimization of the displayed model leads to a structure with alkyl chains pushed out of the siloxy planes,
305 thus increasing the closest inter-chain distance to approximately 4 Å: similar to the usually observed inter-chain
306 distance in such systems and contributing to the stability of the organic layer [51]. Therefore, as the
307 silsesquioxanes are supposed to be composed of stacked, more or less plane parallel layers, the most plausible
308 microscopic model representing the **P1** structure is the first. Accordingly, steric constraints from Van der Waals
309 diameters of C and its bonded H (i.e., 3.5 and 2.5 Å, respectively) prevent the build-up of such dense structure
310 [52].

311



312 **Figure 9.** Example of an alternative microscopic model for the structure **P1**. The too short inter-chain distances
313 prevent lateral packing of alkyl chains, making this model impossible.

314

315 4. Conclusion

316 The formation of hybrid film with a hierarchical structure and uniform macroscopic morphology (film) was
317 achieved by the self-directed sol-gel photopolymerization of a dissymmetric bis-silylated alkyltrimethoxysilane

318 precursor (**1**). At microscopic level, well-defined crystallites were generated within the film, consisting
319 themselves of nanolayered organosilica. The mesostructure organization was deduced through the combination
320 of experimental XRD, ²⁹Si solid-state NMR data and molecular modeling. The most likely mesoscopically
321 organized structure was determined by taking into account steric restrictions which arise when the Si-O-Si bond
322 distance is less than the van der Waals radii of the alkyl chains. In **P1**, the most probable structure consists of bi-
323 layered stack of slightly interpenetrated highly trans C₈H₉ chains, with a single “hybrid” chain based on a
324 repeating –O-Si-CH₂ unit. **P1** had a higher level ordering than its symmetric analogue **P2**. Additionally, its
325 mesostructure was also more thermally stable to disorder than **P3** formed with the mono-silylated analogue
326 despite a lower level of condensation. The apparent contradiction can be understood on the basis that the
327 dominant process governing mesostructure stability is the higher fraction of crystalline phase. Future studies will
328 focus on the self-assembly of novel dissymmetric bisilylated precursors without surfactant by varying the position
329 of the alkoxy groups onto the hydrocarbon backbone. In addition, the self-assembly study of dimeric
330 organosilane structures containing two hydrophobic groups (hydrocarbon chain) and two hydrophilic groups
331 (Si(OH)₃ groups) in the molecule may be of interest because of their strong analogy with gemini surfactants.

332

333 Acknowledgements

334 Dr. Lingli Ni would like to thank the financial support from the National Natural Science Foundation of
335 China (No. 51503072), Natural Science Foundation of Jiangsu Province (No. BK20150419) and Six Talent
336 Peaks Project in Jiangsu Province (No. 2016XCL010).

337

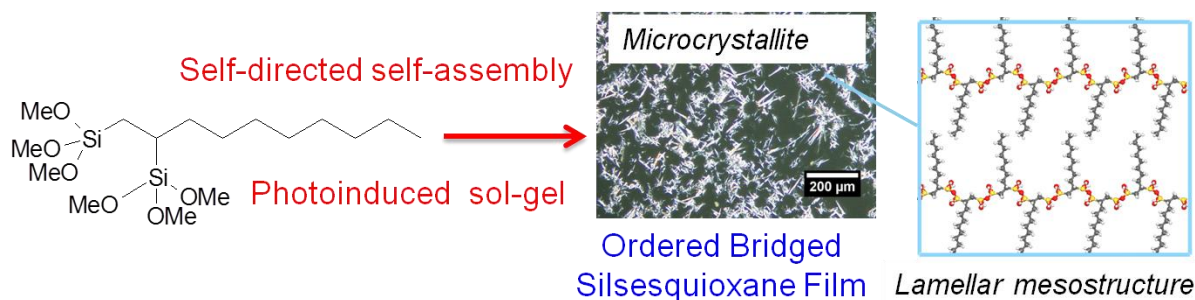
338 References:

- 339 1. Kumar C (2010) Nanostructured Thin Films and Surfaces (Wiley-VCH, Weinheim).
- 340 2. Wang J, Cheng Q, Tang Z (2012) Chem Soc Rev 41(3):1111-1129.
- 341 3. Gin D, Bara J, Noble R, Elliott B (2008) Macromol Rapid Commun 29(5):367-389.
- 342 4. Yan F, Texter J (2006) Adv Colloid Inter Sci 128-130:27-35.
- 343 5. Brinker CJ (2004) MRS Bulletin 29(9):631-640.
- 344 6. Wan Y, Zhao D (2007) Chem Rev 107(7):2821-2860.
- 345 7. Innocenzi P, Malfatti L (2013) Chem Soc Rev 42(9):4198-4216.
- 346 8. Moreau JJE, Vellutini L, Wong Chi Man M, Bied C, Bantignies JL, Dieudonné P, Sauvajol JL (2001) J Am
347 Chem Soc 123(32):7957-7958.
- 348 9. Shimojima A, Kuroda K (2003) Angew Chem Int Ed 42(34):4057-4060.
- 349 10. Huo Q, Margolese DI, Stucky GD (1996) Chem Mater 8(5):1147-1160.
- 350 11. Fujita S, Inagaki S (2008) Chem Mater 20(3):891-908.
- 351 12. Mehdi A, Reye C, Corriu R (2011) Chem Soc Rev 40(2):563-574.
- 352 13. Chemtob A, Ni L, Croutxé-Barghorn C, Boury B (2014) Chem Eur J 20(7):1790-1806.
- 353 14. Yusa S, Ohno S, Honda T, Imoto H, Nakao Y, Naka K, Nakamura Y, Fujii S (2016) RSC Adv
354 6(77):73006-73012.
- 355 15. Bantignies JL, Vellutini L, Maurin D, Hermet P, Dieudonné P, Wong Chi Man M, Bartlett JR, Bied C,
356 Sauvajol JL, Moreau JJE (2006) J Phys Chem B 110(32):15797-15802.
- 357 16. Dieudonné P, Wong Chi Man M, Pichon BP, Vellutini L, Bantignies JL, Blanc C, Creff G, Finet S,
358 Sauvajol JL, Bied C, Moreau JJE (2009) Small 5(4):503-510.
- 359 17. Boury B, Corriu R (2003) Chem Rec 3(2):120-132.
- 360 18. Ruiz-Hitzky E (2005) Organic-Inorganic Materials: From Intercalation Chemistry to Devices. Functional
361 Hybrid Materials (Wiley-VCH Verlag GmbH & Co. KGaA), pp 15-49.
- 362 19. Mehdi A (2010) J Mater Chem 20(42):9281-9286.
- 363 20. Creff G, Pichon BP, Blanc C, Maurin D, Sauvajol JL, Carcel C, Moreau JJE, Roy P, Bartlett JR, Wong Chi
364 Man M, Bantignies JL (2013) Langmuir 29(18):5581-5588.
- 365 21. Cojocariu AM, Cattoen X, Le Parc R, Maurin D, Blanc C, Dieudonné P, Bantignies JL, Wong Chi Man M,
366 Bartlett JR (2016) Phys Chem Chem Phys 18(11):7946-7955.

- 367 22. Carlos LD, de Zea Bermudez V, Amaral VS, Nunes SC, Silva NJO, Sá Ferreira RA, Rocha J, Santilli CV,
368 Ostrovskii D (2007) *Adv Mater* 19(3):341-348.
369 23. Shimojima A, Sugahara Y, Kuroda K (1998) *J Am Chem Soc* 120(18):4528-4529.
370 24. Shimojima A, Sugahara Y, Kuroda K (1997) *Bull Chem Soc Jpn* 70(11):2847-2853.
371 25. Moreau JJE, Vellutini L, Wong Chi Man M, Bied C, Dieudonné P, Bantignies JL, Sauvajol JL (2005)
372 *Chem Eur J* 11(5):1527-1537.
373 26. Nunes SC, Bürglová K, Hodačová J, Ferreira RAS, Carlos LD, Almeida P, Cattoën X, Wong Chi Man M,
374 de Zea Bermudez V (2015) *Eur J Inorg Chem* 2015(7):1218-1225.
375 27. Croissant JG, Cattoën X, Durand JO, Wong Chi Man M, Khashab NM (2016) *Nanoscale* 8:19945-19972.
376 28. Rosen MJ (2004) *Surfactants and Interfacial Phenomena* (John Wiley & Sons, Inc.).
377 29. Shimojima A, Liu Z, Ohsuna T, Terasaki O, Kuroda K (2005) *J Am Chem Soc* 127(40):14108-14116.
378 30. Shimojima A, Goto R, Atsumi N, Kuroda K (2008) *Chem Eur J* 14(28):8500-8506.
379 31. Kuroda K, Shimojima A, Kawahara K, Wakabayashi R, Tamura Y, Asakura Y, Kitahara M (2014) *Chem*
380 *Mater* 26:211-220.
381 32. Shimojima A, Kuge H, Kuroda K (2011) *J Sol-Gel Sci Technol* 57(3):263-268.
382 33. Temtsin G, Asefa T, Bittner S, Ozin GA (2001) *J Mater Chem* 11(12):3202-3206.
383 34. Yang Q, Kapoor MP, Inagaki S (2002) *J Am Chem Soc* 124(33):9694-9695.
384 35. Song LD, Rosen MJ (1996) *Langmuir* 12(5):1149-1153.
385 36. Katagiri K, Hashizume M, Ariga K, Terashima T, Kikuchi J (2007) *Chem Eur J* 13(18):5272-5281.
386 37. Menger FM, Keiper JS (2000) *Angew Chem Int Ed* 39(11):1906-1920.
387 38. Chemtob A, Ni L, Croutxe-Barghorn C, Demarest A, Brendle J, Vidal L, Rigolet S (2011) *Langmuir*
388 27(20):12621-12629.
389 39. Mayo SL, Olafson BD, Goddard WA (1990) *J Physl Chem* 94(26):8897-8909.
390 40. Oviatt H, Shea Kenneth, James S (1993) *Chem Mater* 5(7):943-950.
391 41. Baney RH, Itoh M, Sakakibara A, Suzuki T (1995) *Chem Rev* 95(5):1409-1430.
392 42. Ben F, Boury B, Corriu RJP, Le Strat V (2000) *Chem Mater* 12(11):3249-3252.
393 43. Arkles B, Pan Y, Larson GL, Singh M (2014) *Chem Eur J* 20(30):9442-9450.
394 44. Ni L, Chemtob A, Croutxe-Barghorn C, Brendle J, Vidal L, Rigolet S (2012) *J Phys Chem C*
395 116(45):24320-24330.
396 45. Ni L, Chemtob A, Croutxe-Barghorn C, Brendle J, Vidal L, Rigolet S (2012) *J Mater Chem* 22:643-652.
397 46. Fujii K, Fujita T, Iyi N, Kodama H, Kitamura K, Yamagishi A (2003) *J Mater Sci Lett* 22:1459-1461.
398 47. Bourlinos AB, Chowdhury SR, Jiang DD, An YU, Zhang Q, Archer LA, Giannelis EP (2005) *Small* 1:80-
399 82.
400 48. Fujii K, Kodama H, Iyi N, Fujita T, Kitamura K, Sato H, Yamagishi A, Hayashi S (2013) *New J Chem*
401 37:1142-1149.
402 49. Okamoto K, Goto Y, Inagaki S (2005) *J Mater Chem* 15(38):4136-4140.
403 50. Stevens MJ (1999) *Langmuir* 15(8):2773-2778.
404 51. Bonhomme F, Kanatzidis MG (1998) *Chem Mater* 10(4):1153-1159.
405 52. Wang R, Baran G, Wunder SL (2000) *Langmuir* 16(15):6298-6305.

406
407
408

Graphical abstract



409